DOI: 10.1590/2317-4889201620160021

ARTICLE

A mineral potential mapping approach for supergene nickel deposits in southwestern São Francisco Craton, Brazil

Uma abordagem de mapeamento de potencial mineral dos depósitos de níquel supérgeno do sudeste do Cráton do São Francisco

João Gabriel Motta[1]*, Ilio Rodarte Faria Júnior[2]

ABSTRACT: Southwestern São Francisco Craton makes limit with Brasília thrust-fold belt and involves rocks from Archean to formed during the Brasiliano-Pan Africano Neoproterozoic event, including a mafic-ultramafic belt (Morro do Ferro Greenstone Belt) hosted along the Archean counterpart. This greenstone belt hosts two-nickel deposits (Morro do Níquel and O'Toole, respectively silicate and sulfide types) and occurrences. This study applies an empirical-conceptual model for lateritic nickel deposits formation into geographic information systems with aerogeophysical data (magnetic and gamma-spectrometry) and digital elevation models (terrain relief and slope). Our contribution aims for nickel deposits favorability mapping using a simple mathematical operator over a supporting spatial database translating the conceptual exploration model into evidential layers for geological processes involved on deposit formation. Evidential layers constructed for identification of elements pertaining the supergene nickel mineral system are given by analytic signal amplitude maps, thorium over potassium ratio images, and digital elevation models and slope maps, derived from shuttle radar topography mission digital elevation models. Evidential layers integration through binary layers algebraic sum identified effectively known deposits and occurrences with its outputs highlighting possibilities for unknown resources in this under-explored terrain.

KEYWORDS: prospection; mineral exploration; geographic information systems.

RESUMO: *A região sudeste do estado de Minas Gerais encontra-se no limite do Cráton do São Francisco com um sistema de dobras, empurrão e cisalhamento formados no Neoproterozóico no evento Brasiliano-Pan Africano, com envolvimento de assembleias do arqueano até essa idade e inclui associação de rochas máficas- ultramáficas (Greenstone Belt Morro do Ferro). A esta unidade arqueana estão associados depósitos minerais de níquel (Morro do Níquel e O'Toole, supérgeno silicatado e sulfetado, respectivamente) e ocorrências minerais. Neste estudo se propõe a aplicação de um modelo conceitual empírico de formação de depósitos de níquel laterítico para implementar técnicas de geoprocessamento sobre dados aerogeofísicos (magnéticos e gama-espectrométricos), modelos digitais de elevação (topografia e declividade de terreno) e geologia para a identificação de áreas prospectivas no Greenstone Belt Morro do Ferro. A interpretação e o processamento desses dados permitiram a produção de planos de informação que registrassem processos geológicos necessários para a formação desses depósitos. A integração deles por um modelo de soma algébrica de camadas binárias possibilitou o mapeamento de zonas de potencial mineralização em níquel de forma eficaz, identificando mineralizações conhecidas e até mesmo delineando novos tratos de possível mineralização em um terreno ainda pouco explorado.*

PALAVRAS-CHAVE: *prospecção; exploração mineral; sistemas de informação geográfica.*

[1]Instituto de Geociências, Universidade Estadual de Campinas – UNICAMP, Campinas (SP), Brazil. E-mail: *jgmotta@yahoo.com.br*

[2]Programa de Pós-Graduação em Geociências e Meio Ambiente, Universidade Estadual Paulista Júlio de Mesquita Filho – UNESP, Rio Claro (SP), Brazil. E-mail: *rdt.ilio@gmail.com*

*Corresponding author.

Manuscript ID: 20160021. **Received in:** 01/28/2016. **Approved in:** 05/14/2016.

INTRODUCTION

Archean greenstone belts host important nickel reserves along ultramafic/mafic plutonic and volcanic systems, including its subsequent deformation products, through metamorphic/hydrothermal alteration redistribution, and frequently its weathering products (Golightly 1979, Marsh *et al.* 2013, Butt & Cluzel 2013). Despite contribution from sulfide deposits in nowadays economics, the lateritic resources play an important role on nickel reserves with tenors varying from a 1.0% average with abnormal higher grades up to 3% Ni (Marsh *et al.* 2013, Butt & Cluzel 2013). South America complies with 8% of the world nickel resources with lateritic counterparts accounting for the most of it, in contrary to the common major input from sulfide ores (Peck & Huminick 2016).

The São Francisco Craton presents a complex tecto-no-stratigraphic association of trondjhemite-tonalitic-granodioritic gneisses and volcano-sedimentary belts including an Archean metavolcano sedimentary sequence along its limits with Tocantins Structural Province (Teixeira & Danni 1979, Hasui 2010). This metavolcanic sequence, named Morro do Ferro Greenstone Belt (MFGB), hosts two nickel deposits along its mafic-ultramafic members, as follows: a silicate- supergene mine (Morro do Níquel MNi mine), and a poly-metallic komatiite-hosted Ni-Cu-Co PGE sulfide deposit (O'Toole, Brenner *et al.* 1990). The greenstone belt sequence received considerable exploration interest up to 1990s, including exploration for precious metals, with little activities since then, and extensive prospective belts being undeveloped (Brenner *et al.* 1990, Feola 2004). Recent geologic remote sensing and geomorphological observations by Faria Jr. (2015) pointed out towards unexplored nickel endowment along the MFGB, despite that the terrain passed through diverse exploration cycles. Given its potential and areal extension, the greenstone belt is suitable for regional remote sensing applications and integration on public databases towards vectoring potential areas.

Mineral potential mapping applications encompasses probabilistic methods for spatial distribution modelling through data- or knowledge-driven approaches; the later relying on expert information based modelling of the targeted phenomena (Carranza 2011). Both approaches are useful depending on data base availability, prior knowledge and expert conceptual background (Bonham-Carter 1994). Prospectivity analysis for nickel systems are common for sulfide-bearing mineralization, from magmatic to hydrothermal ones (Porwal *et al.* 2010, Markwitz *et al.* 2010, Lisitsin *et al.* 2013, Andrade *et al.* 2014) with little focus on supergene systems, which counts only in Carranza *et al.* (1999) work, that followed Golightly (1979) conceptual model for ore formation. In this study, we apply a knowledge-driven system with a simple mathematical operator, introducing geophysical evidential layers in a restricted database context, following a conceptual supergene nickel-ore formation given by aspects on the classical model by Golightly (1981) and further improvements (Brand *et al.* 1998, Marsh & Anderson 2011, Marsh *et al.* 2013).

As the MFGB endures a long time under-exploration, we present here an update on its potential, highlighting the need of more research on its evolution and metallogenesis, and the shortage on public exploration data. Therefore, looking forward the understanding of mineral deposits distribution in MFGB and improving its exploration attractiveness, we conducted an application of geoprocessing techniques on geophysical data and digital elevation models to assess mineral potential for supergene nickel deposits. Moreover, it still does not count on a regional mineral potential mapping evaluation for nickel (or whatever minerals).

GEOLOGY BACKGROUND

Study area takes place on southwestern São Francisco Craton (Archean-Paleoproterozoic) limits with the Neoproterozoic Tocantins Structural Province (Almeida *et al.* 1981) (Fig. 1). The São Francisco Craton surpassed subduction during west Gondwana assembly in the time of the Brasiliano-Pan Africano event, with destruction of its marginal basins and construction of Neoproterozoic fold and shear belts in its surroundings (Almeida *et al.* 1981, Zanardo 1992, Valeriano *et al.* 2008). São Francisco Craton is given in the area by a series of metagranitoids and banded biotite-amphibole-gneisses (Zanardo 1992) that lies in tectonic contacts with MFGB (Teixeira 1978), a mixed meta-volcanosedimentary belt with mafic-ultramafic rocks in a WNW-ESE to E-W trend (Feola 2004), and the Neoproterozoic Araxá Group (Simões 1995), with abundant siliciclastics and minor meta-mafics. MFGB presents ultramafic rocks (komatiites), serpentinites and metabasic rocks as amphibole and chlorite schists up to amphibolite facies metamorphism with komatiitic, tholeiitic and minor calc-alkalic parentage, all lithotypes being overprinted by late, retrograde greenschist facies modification (Teixeira & Danni 1979, Szabó 1996, Zanardo 1992, 2003, Carvalho *et al.* 1993). The polycyclic evolution of the terrane register structural fabrics from Paleoproterozoic events on São Francisco Craton overprinted by the Neoproterozoic fabrics and metamorphism (Valeriano *et al.* 2008, Hasui 2010) along the large-scale Campo do Meio Shear Belt, which promotes a NW-SE fabric (Morales 1993).

The Neoproterozoic Araxá Group consists in a metasedimentary sequence thrusted up over the craton, given by psamopelites, pelites, graywackes and calc-silicate rocks with minor volcanic and volcaniclastic terms (Zanardo *et al.* 1990, Simões 1995). This assemblage outcrops in an East-West trending structure with a late tectonic low-angle shearing foliation (Passos Nappe, Simões 1995) that grades into a high-angle fabric further south.

Discussion over MFGB genesis and evolution is not recent and points out towards two hypotheses: that this association presents (truly) a greenstone belt association or at least a part of a dismembered one, or it represents an ophiolite complex (Teixeira & Danni 1979, Brenner *et al.* 1990, Carvalho *et al.* 1993, Szabó 1996, Zanardo *et al.* 2006, Lima 2014). Faria Jr. (2011) argues that Morro do Níquel ultramafics, previously considered part of the MFGB, have no similarities to greenstone belt associations and lacks definite identification of its origin. Widespread magnetite presence is described in those lithotypes (Brenner *et al.* 1990, Zanardo 1992, Carvalho *et al.* 1993, Szabó 1996, Feola 2004), including its preservation on weathered profiles (Oliveira *et al.* 1998), thus aiding these rocks identification on magnetic data. As for gamma-spectrometric surveys, Potassium (K) is related in concentrations up to 1% (Feola 2004, Lima 2014) including expressive K leaching on weathering profiles (Oliveira *et al.* 1998), and Thorium (Th) is reported as lower than 3 ppm in equivalent concentration (Lima 2014).

Elevation in the area ranges from 703 to 1,346 m above sea level, and a differential relief dissection is present. Elongated convex-concave hills and mountains in homogeneously eroded patterns with inter-fluvial flats dominate the geomorphology, whereas other portions present highly developed dissection with higher erosion rates exposing less-weathered bedrock (RADAMBRASIL 1983). This heterogeneous relief dissection represents a multi-event erosion history, presenting highly-evolved ferruginous concretions along flat-topped regional highs developed in a Post-Cretaceous evolution with strong structural and lithology control, and advanced erosion surface on higher order streams (Oliveira 1990, Oliveira *et al.* 1992).

THE CONCEPTUAL FRAMEWORK FOR LATERITIC NICKEL DEPOSITS FORMATION

Supergene concentrations play an important role on nickel market, corresponding to 60% of world's supply (Butt & Cluzel 2013), also as important contributors to

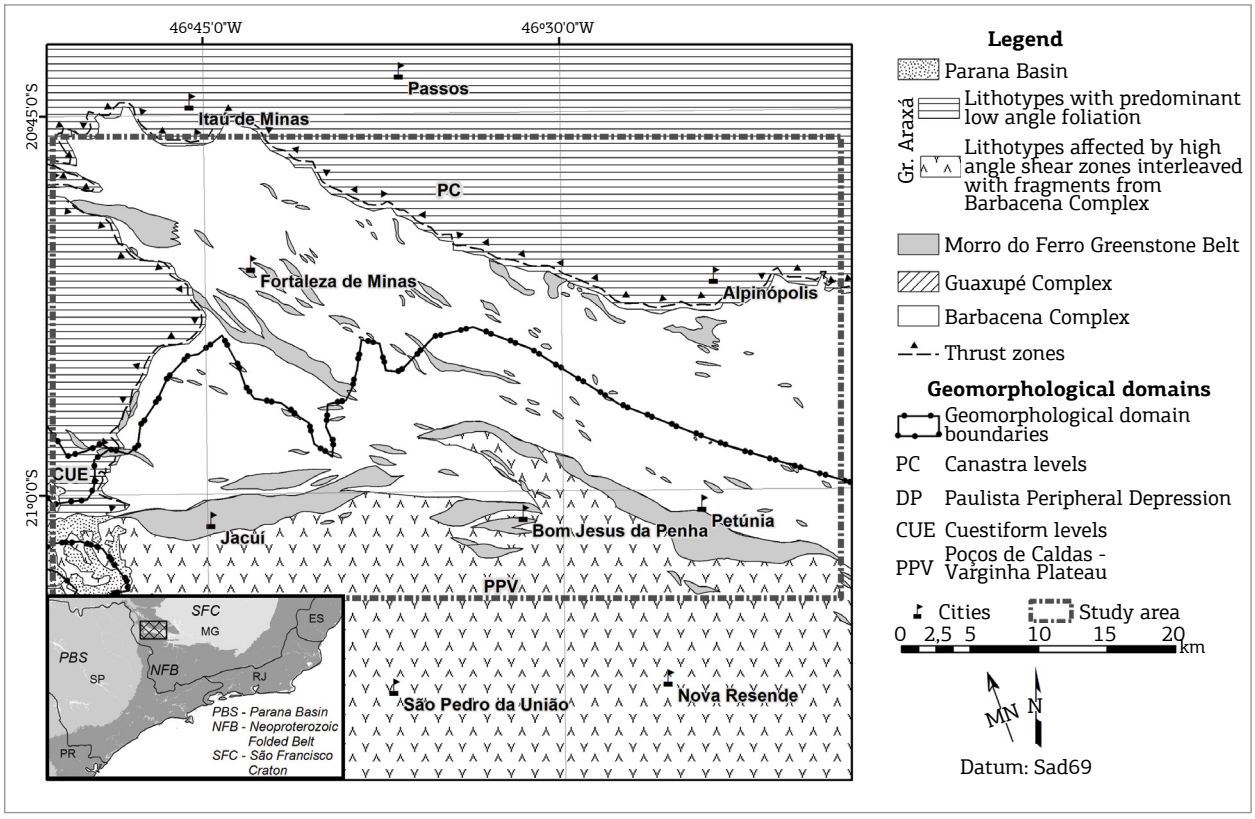

Figure 1. Subject area outline with geological and geomorphological framework, and regional tectonic and political setting (inset, lower left). Geology is adapted from Zanardo (2003), and geomorphology elements from RADAMBRASIL (1983).

the cobalt, platinum group elements and copper global budget, deriving mainly from activities in New Caledonia, Australia, Indonesia and Cuba (Marsh *et al*. 2013). Deposits shares similarities from parent rock to the weathering profile, despite remarkable differences on climatic conditions limits its formations up to 20º from the Equator and occurring over diversely originated mafic/ultramafic bedrock (Marsh *et al*. 2013, Butt & Cluzel 2013).

Despite mineralogical and classification differences between mafic-ultramafic rocks, from plutonic to extrusive counterparts, these rocks are (overall) suitable for supergene nickel enrichment, and to other geochemically similar metals, with serpentinites being the most common parent rock (Golightly 1981, Oliveira *et al*. 1992, Brand *et al*. 1998, Marsh & Anderson 2011). Parent rock composition represents primary control on ore formation, as the rock under weathering must have minerals capable of releasing nickel from its structure and capturing it from subsurface fluids (Brand *et al*. 1998), like olivine, pyroxenes and amphiboles (Lelong *et al*. 1976). Highly suitable lithotypes are, as follows: dunites, peridotites, harzburgites and wehrlites on ophiolite sequences from both Alpine and obducted types on large-scale folding belts; olivine-rich komatiites (like the ones in MFGB); and banded mafic-ultramafic intrusions on Pre-Cambrian basement (Brand *et al*. 1998).

An important stage on supergene nickel concentration is lateritic profile onset over these lithotypes and its preservation from erosion. Mineralization is given by a highly-variable association of Fe-(Mn, Ni, Co) oxides, Ni-Mg-(Co) hydrous silicates, amorphous silica, serpentine, smectites and other clay mineralogy, also (Fe, Mg, Ca, Mn) carbonates and goethite, depending mainly on parent rock mineralogy, climate settings and its temporal evolution (Brand *et al*. 1998, Marsh & Anderson 2011). Those lateritic concentrations are mainly associated with table-like landforms, remainders of previous palaeo-weathering surfaces topped by concretionary latosols with an *armoring* effect preventing profile erosion and element dispersal (Melfi *et al*. 1980, Oliveira *et al*. 1992).

The weathering process comprises geochemical and geomorphological landscapes with a long-term evolution that controls the ions mobilization along the profile, its deposition on the proper sites and preservation along the time, with most concentrations being formed on Phanerozoic Eon over Archean to younger bedrock (Marsh & Anderson 2011, Butt & Cluzel 2013). Butt and Cluzel (2013) group Ni-laterite deposits in four types, as follows: lateritic regolith, hydrous Mg-silicate deposits, clay silicate type, and oxide deposits. This classification varies from the most widespread Ni enrichment in the profile, Ni-hosting mineralogy, development stage and climatic conditions.

Supergene nickel concentrations in Brazil were reviewed by Melfi *et al*. (1980), Oliveira (1990) and Oliveira *et al*. (1992), highlighting the quite conformable ore-forming environments and distribution along tropical climate. Taufen and Marchetto (1989) describes Ni, Cu, Co and Platinum Group Elements enrichment over primary sulfide ore in O'Toole deposit with strong leaching of the sulfides and host rock, secondary sulfide crystallization and Ni depletion from the uppermost levels to the saprolite and bedrock leading to gossan formation similar to the profiles on the western Australian nickel fields. Faria Jr. (2011, 2015) pointed out towards important structural control on development of Ni-bearing supergene ores in Morro do Níquel and two other places along the MFGB – in Bom Jesus da Penha (BJP), along expressive ultramafic rock lenses, and in Jacuí, formed over less representative bodies of serpentinite bedrock.

This conceptual framework serves for developing a knowledge-driven approach for lateritic nickel deposits exploration along the MFGB, based on spatial features identification on the digital dataset evidential layers/maps that relates to the necessary processes for ore formation.

SPATIAL DATABASE AND METHODS

Following the proposed conceptual model for deposits formation and the geology background to the study area, a geoprocessing assessment of remote sensing database has proceeded to map mineral system elements on a database given by:

- aerogeophysical information given by gamma-spectrometric and magnetics data: survey 7 (Patos de Minas–Araxá–Divinópolis, 2006) from Secretary of Economic Development of the State of Minas Gerais (CODEMIG – *Companhia de Desenvolvimento Econômico de Minas Gerais*) with 100 m flight clearance, 400 m survey line spacing on North-South direction, stored in digital media;
- topography data from Shuttle Radar Topography Mission (SRTM) 1 Arc-Second model (30 m spatial resolution);
- regional geological maps from Zanardo (2003) and geomorphology maps from RADAMBRASIL (1983), both digitized from hard media.

Table 1 brings an outline on data processing, evidential map properties and geoprocessing outputs.

Nabighian *et al*. (2005) and Horsfall (1997) assessed magnetics and gamma-spectromectric geophysics fundamentals for data acquisition, processing and interpretation. USGS (2004) described SRTM conception, products and applications.

Analytic signal amplitude (ASA) (Roest *et al.* 1992) was applied on magnetic data to enhance high magnetization areas, considered here as evidence for mafic-ultramafic bedrock according to its common high content on ferromagnetic minerals and common magnetic response (Grant 1985a, 1985b). ASA also enhances areas away from our interest, like non-mafic ultramafic (highly) magnetic bodies, but it is capable of depicting high magnetization zones despite its dimensions, shape and depth (Roest *et al.* 1992, Nabighian *et al.* 2005). According to these premises and the description of widespread magnetic mineralogy on target lithology, we consider high magnetization zones as possible presence of mafic ultramafic rocks, except expressed otherwise from evidences.

Gamma-spectrometric data processing aimed for mapping weathering properties along the landscape through analysis of Th and K distribution according to its different geochemical behaviors, targeting evolved soil horizons over mafic-ultramafic bedrock (Wilford *et al.* 1997, Ulbrich *et al.* 2009, Ferreira *et al.* 2009, Marsh *et al.* 2013). Potassium has greater mobility than Thorium on weathering conditions, presenting higher depletion rates (Wilford *et al.* 1997, Ferreira *et al.* 2009, Ulbrich *et al.* 2009). Thorium has decreased mobility, preferring fixation on hydroxyl-bearing minerals and colloids like newly-formed Fe-Mn oxide-hydroxides in the soils (Dickson & Scott 1997, Ulbrich *et al.* 2009), only moving on highly acidic conditions (Langmuir & Herman 1980, Boyle 1982). Considering the geochemical behavior of these elements, a scenario of K depletion and Th fixing on evolved soils along the outer horizons in lateritic soil profiles (Wilford *et al.* 1997, Dickson & Scott 1997, Ulbrich *et al.* 2009). Thorium over Potassium ratio images can depict this mutual relationship.

SRTM topography data complied with a digital elevation model (DEM) surface and slope maps for comparison to geomorphology information from RADAMBRASIL (1983). Slope calculation is as the gradient of height with map production in ArcGIS by an internal routine on the Spatial Analyst toolbox. Elevation and slope are important in this case as they help describing the lateritic profile preservation stage, also for information regarding water table control (Brand *et al.* 1998). Lateritic nickel deposit by Melfi *et al.* (1980), Oliveira (1990) and Oliveira *et al.* (1992) that higher elevation plains in southeastern Brazil preserves the oldest weathering profiles. Comparing SRTM-derived information to geomorphology and the conceptual supergene-nickel mineralization model led to evidence maps buildup.

Table 1. Information on processing and evidence layers buildup.

<table>
<tr><th>(I) Spatial database building</th><th>Assembling, selecting and integrity check in input data</th><th>Digital elevation model (raster file)</th><th>Magnetic and gamma-spectrometric data (grid file)</th><th>Bedrock geology (polygon)</th></tr>
<tr><td rowspan="7">(II) Data processing</td><td rowspan="5">Information extraction from input data and binary evidence map creation</td><td>(A) DEM surface interpolation</td><td>(A) Magnetic Field Anomaly, Thorium and Potassium equivalent channels interpolation to surface</td><td>(A) Lithotypes spatial distribution evaluation and projection check</td></tr>
<tr><td>(B) Slope and Elevation map calculation from DEM</td><td>(B) Magnetic data analytical signal filtering</td><td>(B) Reprojection and correction</td></tr>
<tr><td>(C) Analysis for interest threshold detection</td><td>(C) Th/K ratio map creation</td><td>(C) Mafic-ultramafic rocks selection</td></tr>
<tr><td rowspan="2">(D) Reclassification into separate binary maps for elevation and slope</td><td>(D) Analysis for interest threshold selection</td><td rowspan="2">(D) Reclassification into binary map</td></tr>
<tr><td>(E) Reclassification into separate binary maps for analytical signal and gamma-ray</td></tr>
<tr><td rowspan="2">Evidence maps</td><td>Areas with slope ≤ 8º</td><td>Areas with ASA > 0.0251 nT/m</td><td rowspan="2">Mafic-ultramafic areas</td></tr>
<tr><td>Areas with height > 900 m</td><td>Areas with Th/K ratio > 26</td></tr>
<tr><td rowspan="2">(III) Data integration</td><td colspan="3">Evidence maps combination through algebraic sum operation.
Comparison with bedrock geology evidence layer and validation criteria.</td></tr>
<tr><td>Output map</td><td colspan="3">Lateritic nickel prospectivity map</td></tr>
</table>

DEM: digital elevation model; Th/K: Thorium/Potassium; ASA: analytic signal amplitude.

Information on mafic-ultramafic rock outcrop comes from Zanardo (2003) map and serves as comparison factor for prospectivity models presented on this paper.

Aerogeophysical data were processed using Geosoft Oasis Montaj 7.5 platform and ESRI ArcMap 10.2 for DEM data. The latter was also used as geographical information system for data integration, analysis and modelling. Evidence layers were resampled into a common 30 m cell size, on Universal Transversal Mercator projection systems in 23S Córrego Alegre Datum. This was necessary for common cartographic projection and cell size compatibility between evidence layers.

Conversion into binary raster

Data analysis and interpretation led to the establishment of four information layers, selected as input predictor maps for prospectivity modelling. These information layers were subsequently converted into binary maps according to specific data ranges, according to criteria as follows.

A given value range in an information layer was selected as representative of interest elements for nickel prospecting. Then, a reclassification of the raster was applied with the absence of the interest range leading to pixel assignment as zero, meanwhile the presence of the interest values leads to its assignment as one. Converting the evidence layers into a binary data space is necessary for subsequent layer integration into a mineral deposit favorability map. Data range statistical analysis to each geophysical data layer allowed definition of interest data ranges, as follows. Defining a lower limit in 0.0251 nT/m for ASA layer (third quartile, from 0.00 to 2.42 nT/m) gives highest magnetization values in the layer, meanwhile for the Th/K ratio layer a value of 26.00, the median from a range between 2.85 and 45.31, is considered to separate values outstanding background. A cut-off height on 900 m for the digital elevation model and an upper limit in 8º for slope was defined representing the higher levels to be under effect of deep laterization and hosting tabular relief zones. Mafic-ultramafic rock outline polygon defines the binary information, as areas inside the polygons give presence and outside them give absence.

Evidence layer integration into prospectivity map

Following evidence layers definition and preparation, its combination into a prospectivity (or favorability) map can take place by a mathematical operator. In this case, the selected operator is algebraic sum, a pixel per pixel operator that sums up a pixel value of each information layer into an output layer – the prospectivity map. This operation gives a range of occurrence probability of a deposit in a given pixel, from zero (absence of evidence in the whole layer dataset) to four (presence of evidence in every layer in the dataset). Carranza *et al.* (1999) applied this integrative technique using different layers; despite its simpler structure, its outcomes have a straightforward interpretation and easily applied in common GIS platforms through raster operations with good-standing results.

This procedure is an intermediate level operator from the restrictive Boolean logic modelling that defines an output of data from zero (total information absence in considered layer space) to one (presence of any/or all evidence layers, depending on operator selection) and a binary index overlay operator (Bonham-Carter 1994). The later depends on weight selection for the evidence layers, presenting subjectivity issues. The algebraic sum presents subjectivity levels arising from evidence layer input, and these evidence layers selected data range. Therefore, it returns a value scale in the final model, allowing ranking these scores. Combinations for a four-fold evidential layer sum are represented in a Venn diagram (Fig. 2), showing up to 16 possibilities for output pixel scoring.

RESULTS AND DISCUSSION

Input evidence layers

Analytic signal amplitude maps

ASA map highlights area's structural grain with long, linear, high- magnetization zones that relates to tectonic domains and specific lithology (Fig. 3). Notably a linear to sinuous NW-SE trend that inflects eastwards to E-W directions and agrees to Campo do Meio shear belt structural fabrics along

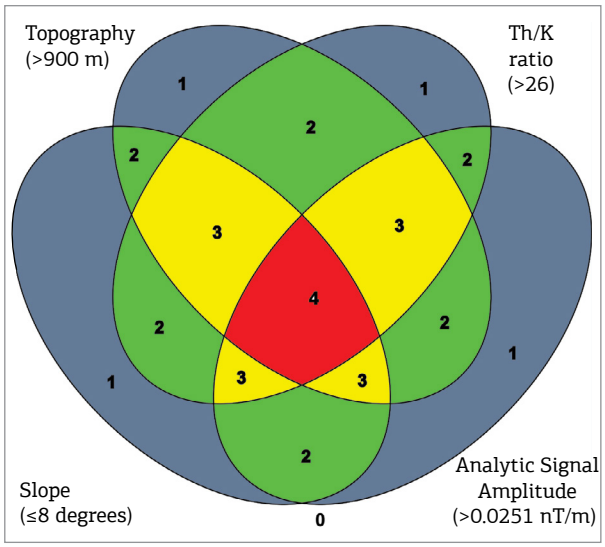

Figure 2. Venn diagram representing score possibilities in four-fold evidential layers algebraic sum into the prospectivity model. Zero stands for absence of evidence, one for its presence.

shear zones (Morales 1993). Besides mafic-ultramafic bodies, high magnetization regions could be related to banded iron formations, deep-seated basic dykes, Phanerozoic intrusive basic rocks (mainly on study area west side) and highly-weathered regions with maghemite or ferruginous concretions along hill tops. Comparing mafic-ultramafic bedrock distribution to ASA maps, it shows that the signal range taken for ASA map transformation into the binary evidence layer (Fig. 4) is compatible (e.g.: ultramafic body east of O'Toole deposit). The binary ASA map (Fig. 4) also shows that some mafic-ultramafic bodies are not highly magnetic as expected (e.g.: ultramafic body hosting BJP occurrences), preventing complete identification of the ultramafic bodies by means of magnetic data, and also highlights potential high magnetization trends conformable to MFGB direction. ASA map usage as evidence layer needs caution considering its performance on mapping target bodies. Target bedrock misidentification or prevention can happen as the region presents polycyclic structural and metamorphic evolution, encompassing retrograde metamorphism on late Brasiliano–Pan African tectonic event, including an uncertain-age serpentinization event, all related to possible magnetite destruction and construction (Carvalho *et al.* 1993, Zanardo 1992, Lima 2014, Faria Jr. 2011).

Gamma-spectrometric maps

Thorium-Potassium ratio maps (Fig. 5) poorly depict bedrock geology, presenting small resemblance on mafic-ultramafic rock outline along the O'Toole deposit vicinity; meanwhile, they present interesting values (greater than 26) on the South-Central region. Their distribution clearly relates to geomorphology,

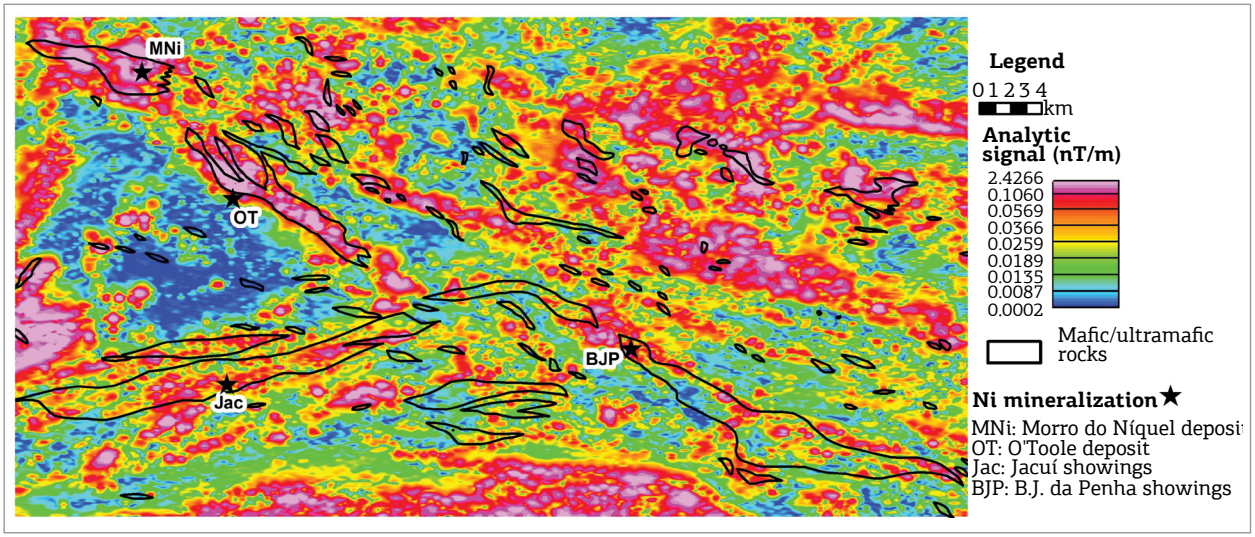

Figure 3. Analytic signal amplitude map, including known nickel mineralization and mafic-ultramafic bedrock outline.

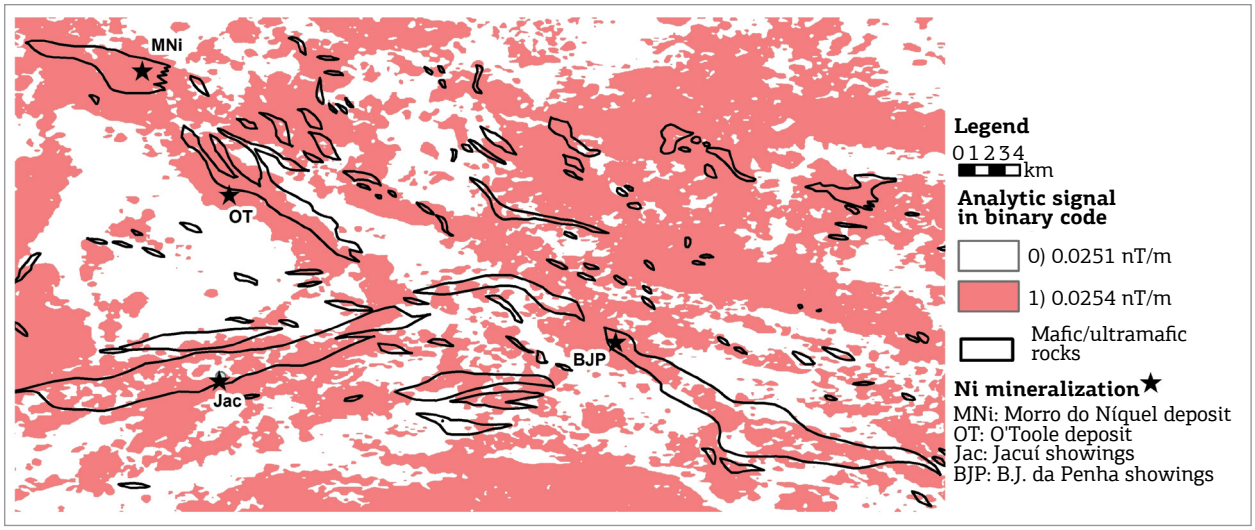

Figure 4. Binary analytic signal amplitude map with known nickel mineralization and mafic-ultramafic bedrock.

as expected, highlighting eroded sections, including low-slope to flat regions. A comparison to DEM (Fig. 6) shows that low Th/K ratio values fairly coincide to the topography lower levels (< 900 m) and probable K fixation in weathering profile. The widely high ratio area in the southern part of the map coincides with an evolved geomorphologic surface in Varginha-Poços de Caldas Plateau upper levels (RADAMBRASIL 1983).

Digital elevation and slope models

Elevation ranges from 703 to 1346 meters above sea level with the greatest heights lying in southern part along NW-SE striking ranges (Fig. 6) that occurs from the center to the north, and a distinct NE-SW plateau on western side. Those NW-SE striking ranges are associated to chemically resistant Neoproterozoic siliciclastic rocks supporting these ridges. Elevation and slope characteristics describe the landforms, giving some insights into the different erosion levels. It is remarkable that the northern part of the study area hosts topographic levels lower than 900 meters, discarded in our binary evidence map (Fig. 6). To consider elevations higher or equal to 900 m as potential for mineralization in the area is in accordance to RADAMBRASIL (1983) description of those as being areas with minor erosion.

Slope ranges from zero to 68º with widespread distribution of tabular/plan relief following the area's structural pattern, including higher slope areas outlining regional plateaus

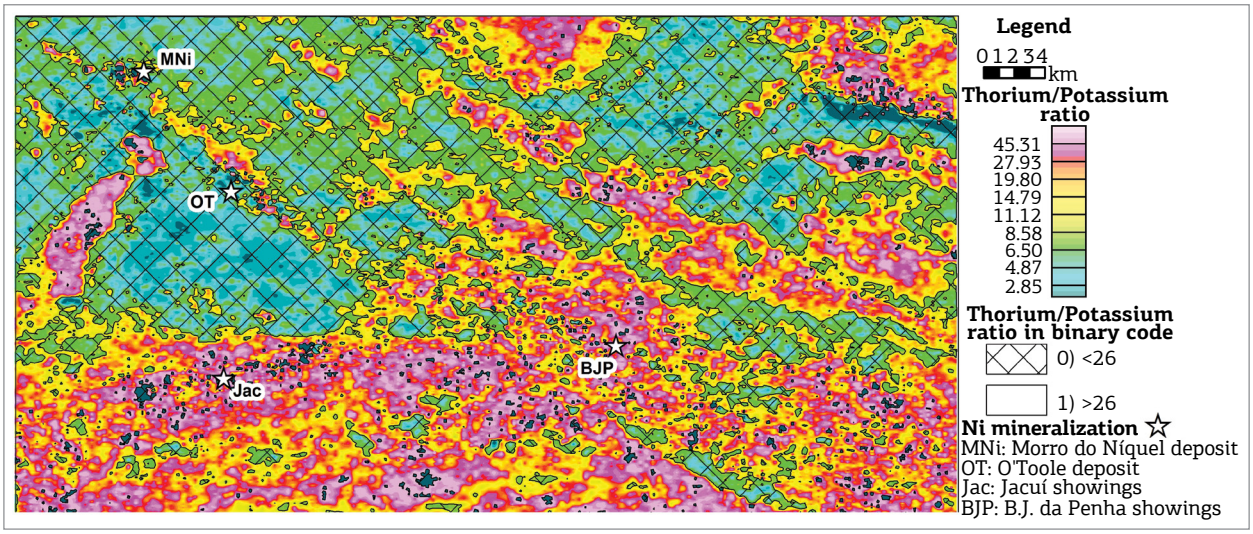

Figure 5. Thorium-Potassium ratio map depicting known nickel mineralization and regions considered in the binary evidence layer.

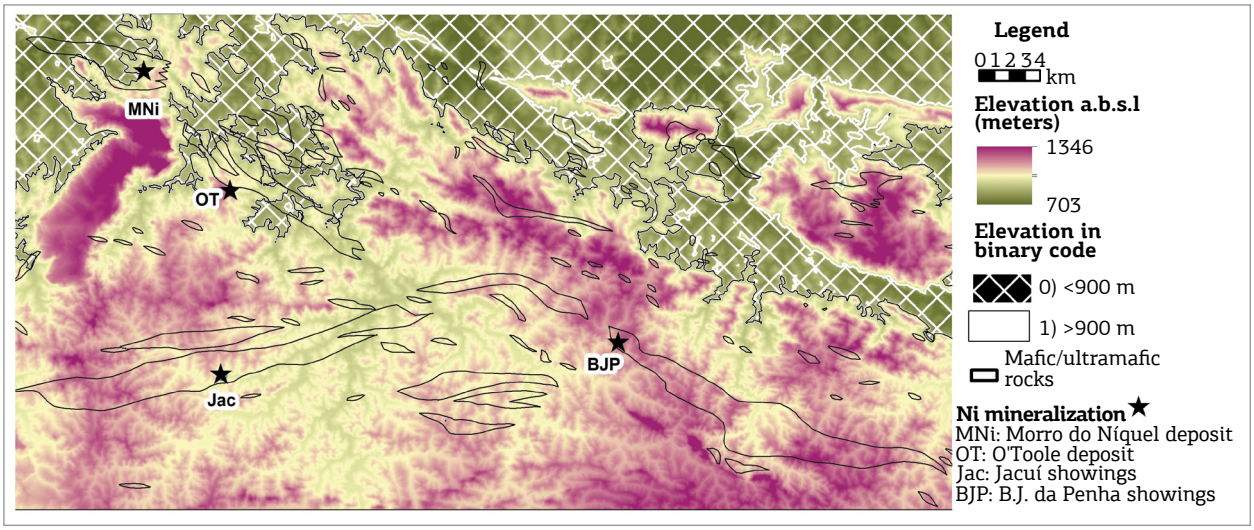

Figure 6. Digital elevation model showing areas considered in binary evidence layer, known nickel mineralization and mafic-ultramafic bedrock geology.

(Fig. 7). Furthermore, areas with slope less or equal to 8º display lower erosion rates (also evident in Th/K ratio maps). Higher slope areas can also preserve an evolved weathering profile, but, according to Melfi *et al.* (1980), the chance to observe them with its better preservation occurs in areas surrounding plan relief levels.

It is worth notice that mass-transfer processes along geomorphology and water table are conformable to lithology and structural patterns. This way, both DEM and slope binary evidential layers mark possible transport trends. DEM and slope maps can be compared to Th/K ratio maps for information on erosion and deposition regional tracts. Despite that main topography outline is in accordance to geological features, it is not possible to establish an immediate relationship between slope and topography maps, and mafic-ultramafic bedrock.

Mineral potential maps and discussion

On the mineral potential map output, each pixel is the sum of the input evidential layers dataset for that pixel, and it is not possible to unveil which input layers contribute to that score, presenting a qualitative value ranging from zero to *n*, as *n* stands for the number of input evidential layers.

A first model that takes into consideration the four evidential layers (ASA, Th/K ratio, elevation and slope) for the whole study area permits inference on possibilities for supergene nickel deposits exploration in a regional context (Fig. 8).

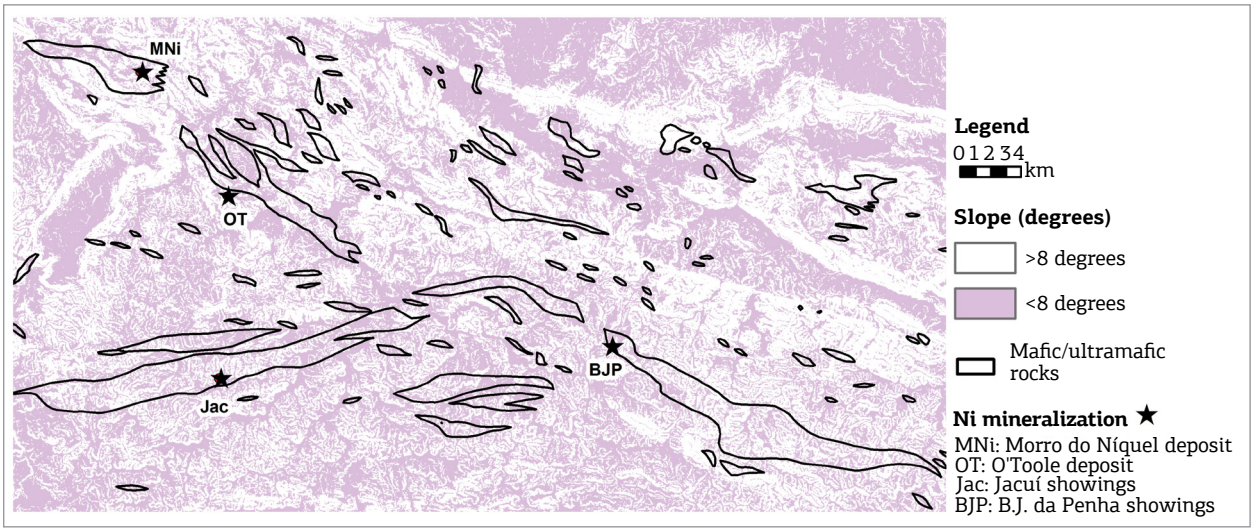

Figure 7. Slope map in binary format for study area, including known nickel mineralization and mafic-ultramafic bedrock outline.

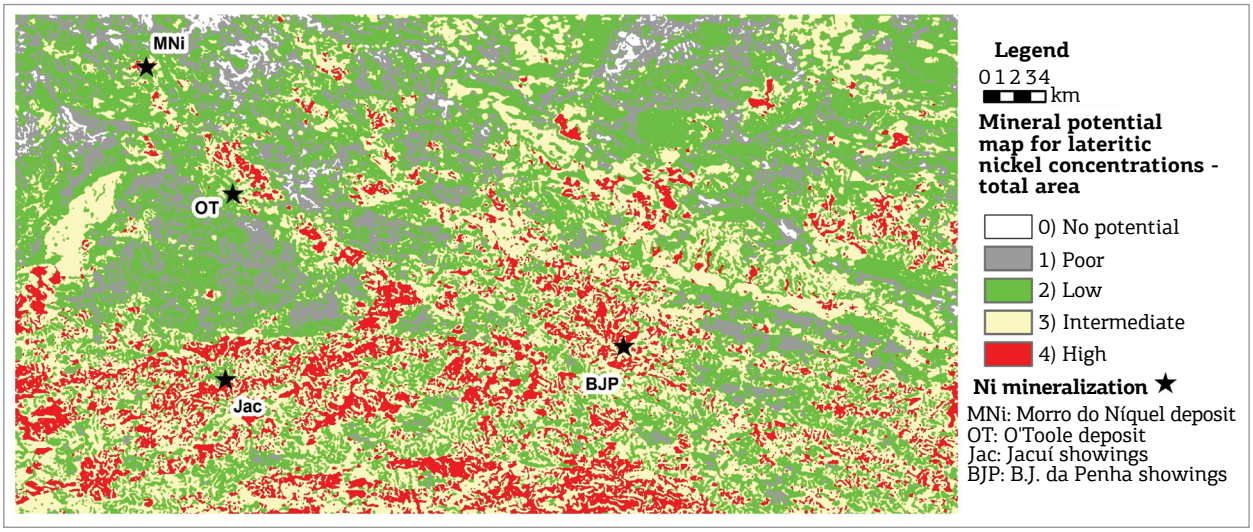

Figure 8. Supergene nickel deposits prospectivity map for the entire study area.

Considering the number of input evidential layers (4) for this model, a score 4 in a pixel is the sum of present evidence in all evidential layers, being the one with higher potential to host a supergene nickel deposit. In contrast, a pixel with score zero is the one in which any of the evidential layers are marked as prospective. Middle-class scores (1 to 3) got the chance to be the combination of any of them, as shows the Venn diagram (Fig. 2), and it is not possible to confirm which layer contributed to that score. It is verifiable from Figure 8 that the prospectivity model delineates several trends according to the structural pattern, as expected given previous examination of evidential layers (ASA, slope and DEM, mainly).

Statistics from this model show that, from a 2000 km² area, about 10% of them are assigned scoring 4, besides 40% scored as poor- to low-potential (scores 1–2). This presents an interesting rate since the screening of these areas presents possible economy on exploration budgets.

A series of high potential areas is highlighted in the southern portion of the area, far south of Jacuí and Bom Jesus da Penha occurrences (Fig. 8), identified as products of higher weathering rates associated higher topography over granulite facies metamorphic rocks with higher magnetite content and Th/K ratios (Campos Neto & Caby 2000, Zanardo *et al.* 2006).

As the area presents considerable geological cartography, a comparison from our first model and known prospective bedrock has been produced (Fig. 9), showing up interesting features as follows. The discontinuous prospective belt is not highly favorable as a whole, with higher potential scores clustering, as expected, as laterization process is a complex process interplay. Inclusion of the ASA evidential layer in this model enhances structural discontinuities, also accounting for introduction of information on magnetic banded iron formations presence as levels amid the mafic-ultramafic rocks, as observed in the MFGB and O'Toole deposit (Brenner *et al.* 1990, Carvalho *et al.* 1993).

It is noticeable that intermediate to higher potential scores map the Morro do Níquel and O'Toole deposits, and Bom Jesus da Penha occurrence, as expected from known mineralization. Despite different mineralization style on O'Toole, it is evident that this processing routine is able to map mafic-ultramafic rocks at least to some point. The Morro do Níquel deposit is mapped as a high potential area for supergene nickel concentrations in agreement to its weathering profile developed over ultramafic bedrock (serpentinite, overall 0.3% nickel grade) with ore grading up to 4% nickel and averaging 1.5 to 2.0%, representing a concentration factor up to 700% from the parent rock (Faria Jr. 2011). At Bom Jesus da Penha area, Faria Jr. (2015) highlights existence of an enrichment factor up to 350% on mottled saprolite formed over chlorite-amphibole schist (1198 ppm Ni), also concentrating cobalt and copper. Besides, this author describes a weathering profile along Jacuí, formed on propitious geomorphologic conditions over possible ultramafic bedrock. In the absence of public regional exploration geochemistry data (stream sediment or whole rock chemistry), we agree that the proper definition of known mineralization along our models serves somewhat as validation.

In the light of different possibilities for scoring in the previous prospectivity model, a second model is

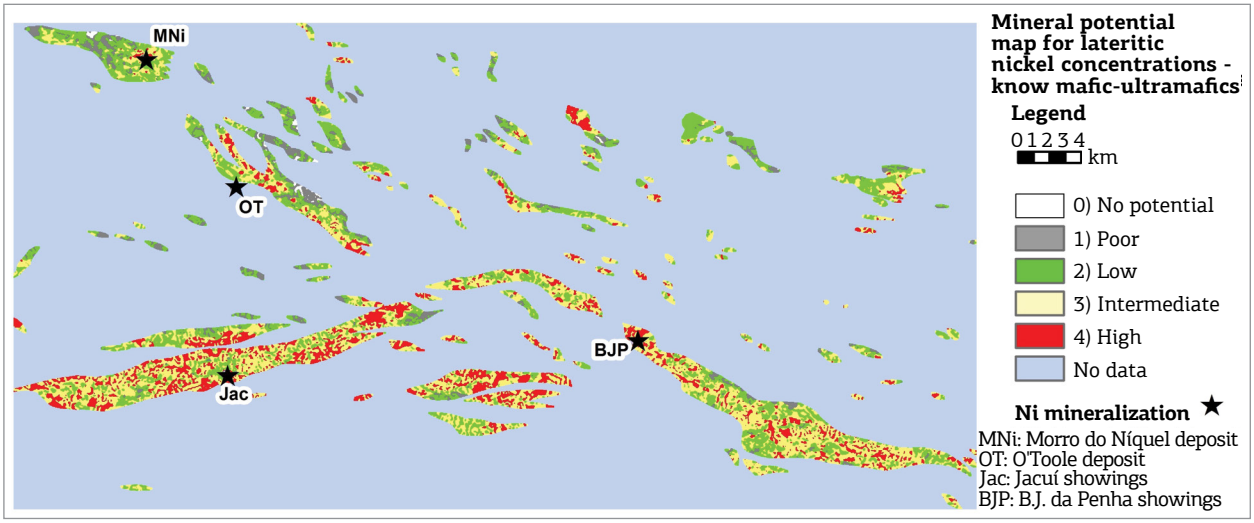

Figure 9. Mineral potential map for supergene nickel deposits in the known mafic-ultramafic bedrock for the ASA-included model.

presented (Fig. 10), accounting only the Th/K ratio, DEM and slope evidential layers over known prospective bedrock areas (35% of the total area) as it presents an important prospectivity control by itself. A considerable change is observed in a comparison from Figure 8 to Figure 9, showing up more continuous higher prospectivity areas, especially in the southern mafic-ultramafic bodies. Known mineralization appears as intermediate to high scores, and BJP defines a big potential areas cluster. Higher potential spots exist on south-central region of the study area, also in an isolated NW-SE small lens-like body in the central-north region.

Statistics from prospectivity scores in the ASA-including model show that 20% of the area scores a high potential level; meanwhile, in the model accounting only for areas with mafic-ultramafic bedrock the areas ranking 4 represents 33% of the total. That said it is feasible that ASA possibly acts as restrictive evidence in the modeling and its exclusion can be considered for a regional scale appraisal for known bedrock. Therefore, it is necessary to supply other evidential layer type to prevent non-target rock inclusion or its misidentification (e.g.: gravity data, optical remote sensing information).

CONCLUSION

This contribution presents a straightforward procedure to convert a conceptual mineral deposit model into an exploration model through simple geoprocessing techniques that help screening and ranking potential areas in regional exploration programs. Concerning restricted data availability and its wide-scale nature, which includes relatively poor data resolution in geophysical data and absence of regional geochemistry data, this application proved itself able to identify regional prospective tracts for supergene nickel deposits in the MFGB. Evidential layers mapping effectiveness is subject to a range of issues like spatial and spectral resolution, survey orientation, data spatial projection and bedrock geological aspects, thus, data set reliability and its proper handling plays an important role. Different evidential layers combinations are possible. Thus, its modifications are subjective in respect of expert decision, like any knowledge-driven approach, as selection of both evidence layers and data range considerations are under its responsibility prior to mathematical integration, as shows the previous example of change into the sum of evidential layers.

Evidence layer integration by algebraic sum on an equal weight basis is a simple and straightforward operator, recommended to relatively simple exploratory models, and this practice also showed its capability in dealing with a restrict spatial database. Therefore, we recommend caution, the use of a well-established conceptual model and field check for feedback, as both overestimation and underestimation play a role.

In more advanced exploration, scenarios counting on more data types (e.g.: stream sediment geochemistry, gravity surveys, mineralogy spectra data) and knowledge over mineralization styles and geological processes, different sorts of evidential layers can be considered, including application of different mathematical operators for integration, possibly reducing subjectivity and improving success rate. Prior

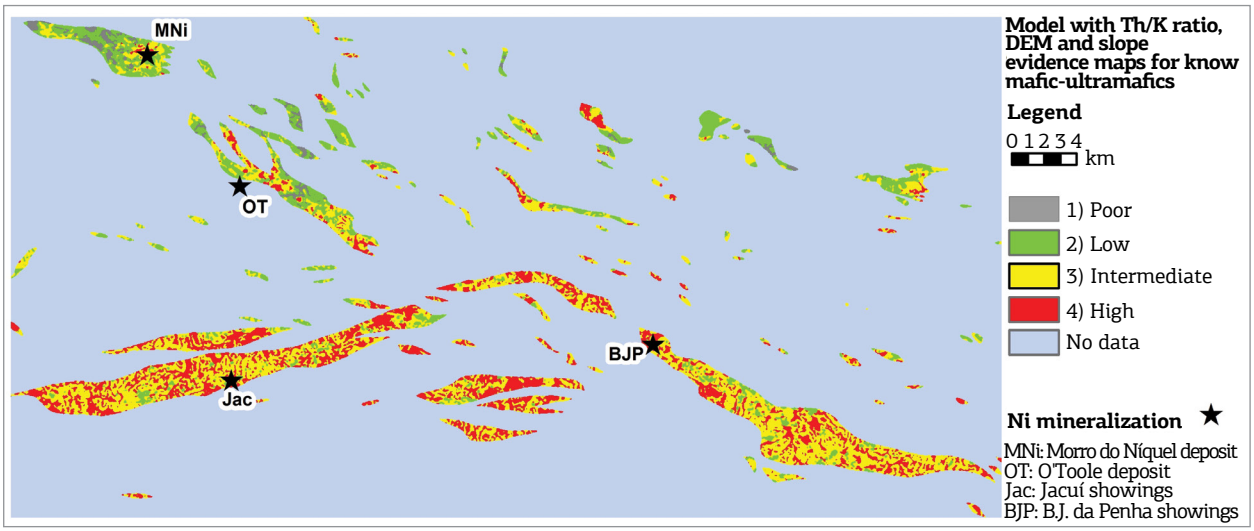

Figure 10. Mineral potential map for supergene nickel deposits in mafic-ultramafic bedrock for the ASA-excluded prospectivity model.

knowledge on regional scale tectonic settings and mineral deposit styles permitted to compare the effectiveness of modelling process proposed here in respect to identification of both mafic-ultramafic host rocks and mineralized spots.

Despite the first target in this practice is to map possible areas with supergene lateritic nickel deposits, it also can track some elements with similar geochemical behavior, like copper and cobalt, including its fresh host rocks (Marsh & Anderson 2011). Nevertheless, availability of public geochemical exploration data would improve detection and validation for the two proposed prospectivity models, also helping on targeting for other elements than nickel.

ACKNOWLEDGEMENTS

Authors are thankful to Norberto Morales for insightful comments and providing computational infrastructure access at Laboratory of 3D Geo-Modelling (*Laboratório de Geomodelagem 3D*) in Universidade Estadual Paulista "Júlio de Mesquita Filho", Rio Claro Campus. J.G.M. is thankful to Carlos Roberto de Souza Filho from Universidade de Campinas (UNICAMP) and E.J.M. Carranza for contributions and stimulus to write this paper. The authors are thankful to the anonymous reviewers for the insighful and careful revision. We also give thanks to CODEMIG for providing access to geophysical data.

REFERENCES

Almeida F.F., Hasui Y., Brito Neves B.B., Fuck R.A. 1981. Brazilian structural provinces: an introduction. *Earth-Science Reviews*, **17**:1-19.

Andrade L.B., Silva A.M., Souza Filho C.R. 2014. Nickel prospective modelling using fuzzy logic on Nova Brasilândia metasedimentary belt, Rondônia, Brazil. *Revista Brasileira de Geofísica*, **32**(3):419-431.

Bonham-Carter G.F. 1994. *Geographic Information Systems for Geoscientists*: Modelling with GIS. Ontario, Pergamon Press, 398 p.

Boyle R.W. 1982. *Geochemical prospecting for Thorium and Uranium deposits*. Developments in Economic Geology, 16. Amsterdam, Elsevier, 498 p.

Brand N.W., Butt C.R., Elias M. 1998. Nickel laterites: classification and features. *Journal of Australian Geology & Geophysics*, **17**(4):81-88.

Brenner T.L., Teixeira N.A., Oliveira J.A.L., Franke N.D., Thompson J.F.H. 1990. The O'Toole nickel deposit, Morro do Ferro Greenstone Belt, Brazil. *Economic Geology*, **85**:904-920.

Butt C.R.M. & Cluzel D. 2013. Nickel laterite ore deposits: weathered serpentinites. *Elements*, **9**:123-128.

Campos Neto M.C. & Caby R. 2000. Terrane accretion and upward extrusion of high-pressure granulites in the Neoproterozoic nappes of southeast Brazil: petrologic and structural constraints. *Tectonics*, **19**(4):669-687.

Carranza E.J.M. 2011. Geocomputation of mineral exploration targets. *Computers & Geosciences*, **37**:1907-1916.

Carranza E.J.M., Mangaoang J.C., Hale M. 1999. Application of mineral exploration models and GIS to generate mineral potential maps as input for optimum land-use planning in the Philippines. *Natural Resources Research*, **8**(2):165-173.

Carvalho S.G., Soares P.C., Antônio M.C., Zanardo A., Oliveira M.A.F. 1993. Geologia da sequência vulcano-sedimentar de Alpinópolis (MG). *Revista Brasileira de Geociências*, **23**(1):38-51.

Dickson B.L. & Scott K.M. 1997. Interpretation of aerial gamma-ray surveys – adding the geochemical factors. *Journal of Australian Geology & Geophysics*, **17**(2):187-200.

Faria Jr. I.F. 2011. *Modelo estrutural da mineralização na jazida Morro do Níquel, Pratápolis, MG*. Graduate Thesis, Instituto de Geociências e Ciências Exatas, Universidade Estadual Paulista "Júlio de Mesquita Filho", Rio Claro, São Paulo, Brazil, 80 p.

Faria Jr. I.F. 2015. *Prospecção mineral de alvos potenciais à ocorrência de enriquecimento supergênico de níquel no Greenstone Belt do Morro do Ferro*. MS Dissertation, Instituto de Geociências e Ciências Exatas, Universidade Estadual Paulista "Júlio de Mesquita Filho", Rio Claro, São Paulo, Brazil, 137 p.

Feola J.L. 2004. *Mineralizações auríferas hospedadas na faixa vulcano-sedimentar Jacuí-Bom Jesus da Pena – sudoeste de Minas Gerais*. PhD Thesis, Instituto de Geociências e Ciências Exatas, Universidade Estadual Paulista Júlio de Mesquita Filho, Rio Claro, São Paulo, Brazil, 211 p.

Ferreira F.J.F., Fruchting A., Guimarães G.B., Alves L.S., Martin V.M.O., Ulbrich H.H.G.J. 2009. Levantamentos gamaespectrométricos em granitos diferenciados. II: o exemplo do Granito Joaquim Murtinho, Complexo Granítico de Cunhaporanga, Paraná. *Revista do Instituto de Geociências – USP*, **9***(1):55-72.*

Golightly J.P. 1979. Nickeliferous laterites: a general description. *In*: Evans D.J.I., Shoemaker R.S., Veltman H. (Eds.). *International Laterite Symposium*. New York, Society of Mining Engineers, American Institute of Mining, Metallurgical and Petroleum Engineers, p. 3-23.

Golightly J.P. 1981. Nickeliferous laterite deposits. *Economic Geology*, 75th anniversary volume, 710-735.

Grant F.S. 1985a. Aeromagnetics, geology and ore environments, I. Magnetite in igneous, sedimentar and metamorphic rocks: an overview. *Geoexploration*, **23**:303-333.

Grant F.S. 1985b. Aeromagnetics, geology and ore environments, II. Magnetite and ore environments. *Geoexploration*, **23**:335-362.

Hasui Y. 2010. A grande colisão Pré-Cambriana do sudeste brasileiro e a estruturação regional. *Geociências*, **29**(2):141-169.

Horsfall K.R. 1997. Airborne magnetic and gamma-ray data acquisition. *Journal of Australian Geology & Geophysics*, **17**(2):23-30.

Langmuir D. & Herman J.S. 1980. The mobility of thorium in natural waters at low temperatures. *Geochimica et Cosmochimica Acta*, **44**:1753-1766.

Lelong F., Tardy Y., Grandin G., Trescases J.J., Boulange B. 1976. Pedogenesis, chemical weathering and processes of formation of some supergene ore deposits. *In*: Wolf R.H. (Ed.). *Handbook of stratabound and stratiform ore deposits*, Elsevier, 3, p. 92-173.

Lima F.G. 2014. *Evolução petrogenética das rochas máficas/ultramáficas na área ao sul do Cráton do São Francisco, entre as cidades de Fortaleza de Minas e Jacuí-MG*. MS Dissertation, Instituto de Geociências e Ciências Exatas, Universidade Estadual Paulista "Júlio de Mesquita Filho", Rio Claro, São Paulo, Brazil, 104 p.

Lisitsin V.A., González-Álvares I., Porwal A. 2013. Regional prospectivity analysis for hydrothermal-remobilized nickel mineral systems in western Victoria, Australia. *Ore Geology Reviews*, **52**:100-112.

Markwitz V., Maier W.D., González-Álvares I., Mc Cuaig T.C., Porwal A. 2010. Magmatic nickel sulfide mineralization in Zimbabwe: review of deposits and development of exploration criteria for prospectivity analysis. *Ore Geology Reviews*, **38**:139-155.

Marsh E.E. & Anderson E.D. 2011. *Ni-Co laterite deposits*: U.S. Geological Survey Open-File Report 2011–1259. 9 p.

Marsh E.E., Anderson E.D., Gray F. 2013. Nickel-cobalt laterites: a deposit model. *In*: U. S. Department of the Interior, U. S. Geological Survey. *Mineral deposit models for resource assessment:* U. S. Geological Survey Scientific Investigations Report 2010–5070–H. Chapter H. 38 p. Disponível em: <http://pubs.usgs.gov/sir/2010/5070/h/>. Acesso em: 15 de set. de 2015.

Melfi A.J., Trescases J.J., Oliveira S.M.B. 1980. Les "laterites" nickeliferes du Brésil. *Cahier de Orstom*, Série Géologie, **11**:15-42.

Morales N. 1993. *Evolução tectônica do Cinturão de Cisalhamento Campo do Meio na sua porção ocidental*. PhD Thesis, Instituto de Geociências e Ciências Exatas, Universidade Estadual Paulista "Júlio de Mesquita Filho", Rio Claro, São Paulo, Brazil, 256 p.

Morales N., Carvalho S.G., Choudhuri A., Fiori A.P., Oliveira M.A.F., Rodrigues M.F.B., Soares P.C., Zanardo A. 1983. Geologia das folhas de Fortaleza de Minas, Alpinópolis, Jacuí, Nova Resende, MG. *In*: Simpósio de Geologia de Minas Gerais, 2, Belo Horizonte. *Anais...*, Belo Horizonte: SBG-MG, v. 3, p. 411-422.

Nabighian M.N., Grauch V.J.S., Hansen R.O., La Fehr T.R., Li Y., Peirce J.W., Philips J.D., Ruder M.E. 2005. The historical development of the magnetic method in exploration. *Geophysics*, **70**(6):33ND-61ND.

Oliveira S.M.B. 1990. Estágio atual do conhecimento acerca do minério laterítico de níquel no Brasil e no mundo. *Revista do Instituto Geológico*, São Paulo, **11**(2):49-57.

Oliveira S.M.B., Liguoriimbernon R.A., Blot A., Magat P. 1998. Mineralogia, geoquímica e origem dos gossans desenvolvidos sobre o minério sulfetado de Ni-Cu do depósito de O'Toole, Minas Gerais, Brasil. *Revista Brasileira de Geociências*, **28**(3):295-300.

Oliveira S.M.B., Trescases J.J., Melfi A.J. 1992. Lateritic nickel deposits of Brazil. *Mineralium Deposita*, **27:**137-146.

Peck D.C. & Huminicki M.A.E. 2016. Value of mineral deposits associated with mafic and ultramafic magmatism: implications for exploration strategies. *Ore Geology Reviews*, **72**:269-298.

Porwal A., González-Álvares I., Markwitz V., Mc Cuaig T.C., Mamuse A. 2010. Weights-of-evidence and logistic regression modeling of magmatic nickel sulfide prospectivity in the Yilgarn Craton, western Australia. *Ore Geology Reviews*, **38**:184-196.

RADAMBRASIL. 1983. Ministérios de Minas e Energia. *Levantamento dos recursos naturais* – Folhas SF 23/24, Rio de Janeiro/Vitória, v. 32, 780 p.

Roest W.R., Verhoef J., Pilkington M. 1992. Magnetic interpretation using the 3-D analytic signal. *Geophysics*, **57**:116-125.

Simões L.S.A. 1995. *Evolução tectono-metamórfica da Nappe de Passos, sudoeste de MG*. PhD Thesis, Instituto de Geociências, Universidade de São Paulo, São Paulo, 149 p.

Szabó G.A.J. 1996. *Petrologia da suíte metaultramáfica da seqüência vulcano-sedimentar Morro do Ferro na região de sul a oeste de Alpinópolis, MG (domínio norte do Complexo Campos Gerais)*. PhD Thesis, Instituto de Geociências e Ciências Exatas, Universidade Estadual Paulista "Júlio de Mesquita Filho", Rio Claro, São Paulo, Brazil, 354 p.

Taufen P.M. & Marchetto C.M.L. 1989. Tropical weathering control of Ni, Cu, Co and platinum group element distributions at the O'Toole Ni-Cu sulphide deposit, Minas Gerais, Brazil. *Journal of Geochemical Exploration*, **32**:185-197.

Teixeira N.A. 1978. *Geologia e petrologia e prospecção geoquímica da sequência vulcano-sedimentar Morro do Ferro, Fortaleza de Minas (MG)*. MS Dissertation, Instituto de Geociências, de de Brasília, Brasília, 202 p.

Teixeira N.A. & Danni J.C.M. 1979. Geologia da raiz de um greenstone belt na região de Fortaleza de Minas, Minas Gerais. *Revista Brasileira de Geociências*, **9**(1):17-26.

Ulbrich H.H.G.J., Ulbrich M.N.C., Ferreira F.J.F., Alves L.S., Guimarães G.B., Fuchting A. 2009. Levantamentos gamaespectrométricos em granitos diferenciados. I: Revisão da metodologia e do comportamento geoquímico dos elementos K, Th e U. *Revista do Instituto de Geociências – USP*, Geologia USP Série Científica, **9**(1):33-53.

US Geological Survey – USGS. 2004. *Shuttle Radar Topography Mission*, 1 Arc Second scenes, Unfilled Unfinished 2.0. College Park, Maryland: Global Land Cover Facility, University of Maryland, February 2000.

Valeriano C.M., Pimentel M.M., Heilbron M., Almeida J.C.H., Trouw R.A.J. 2008. *Tectonic evolution of the Brasília Belt*, Central Brazil, and early assembly of Gondwana. *In*: Geological Society, London, Special Publications, v. 294, p. 197-210.

Wilford J.R., Bierwith P.N., Craig M.A. 1997. Application of airborne gamma-ray spectrometry in soil/regolith mapping and applied geomorphology. *Journal of Australian Geology & Geophysics*, **17**(2):201-216.

Zanardo A. 1992. *Análise petrográfica, estratigráfica e microestrutural da região de Guaxupé-Passos-Delfinópolis (MG)*. PhD Thesis, Instituto de Geociências e Ciências Exatas, Universidade Estadual Paulista "Júlio de Mesquita Filho", Rio Claro, São Paulo, Brazil, 270 p.

Zanardo A. 2003. Pesquisa geológica e de matérias-primas do centro nordeste do estado de São Paulo e vizinhanças. Associate professor thesis. Instituto de Geociências e Ciências Exatas, Universidade Estadual Paulista "Júlio de Mesquita Filho", Rio Claro, São Paulo, Brazil, 283 p.

Zanardo A., Morales N., Carvalho S.G. 1990. Evolução metamórfica da porção sul do Cráton Paramirim. *In*: Congresso Brasileiro de Geologia, 36, Natal. *Anais...*, Natal: SBG, v. 4, p. 1945-1951.

Zanardo A., Morales N.; Oliveira M.A.F., Del Lama E.A. 2006. Associação tectono-litológica da paleozona de sutura Alterosa, sudeste do Brasil. *Revista UnG-Geociências*, **5**(1):103-117.